Received: 8 September 2017 | Revised: 23 June 2018 | Accepted: 2 July 2018

DOI: 10.1111/pce.13401

ORIGINAL ARTICLE

WILEY Plant, Cell & Environment

Carbon and oxygen isotope fractionations in tree rings reveal interactions between cambial phenology and seasonal climate

Soumaya Belmecheri[1] | William E. Wright[1] | Paul Szejner[1,2] | Kiyomi A. Morino[1] | Russell K. Monson[1,3]

[1] Laboratory of Tree-Ring Research, University of Arizona, Tucson, Arizona

[2] School of Natural Resources and the Environment, University of Arizona, Tucson, Arizona

[3] Department of Ecology and Evolutionary Biology, University of Arizona, Tucson, Arizona

Correspondence
Soumaya Belmecheri, Laboratory of Tree-Ring Research, University of Arizona, Tucson, AZ 85721.
Email: sbelmecheri@email.arizona.edu

Funding information
Division of Emerging Frontiers, Grant/Award Number: 1065790; Division of Environmental Biology, Grant/Award Number: 1754430

Abstract

We developed novel approaches for using the isotope composition of tree-ring subdivisions to study seasonal dynamics in tree–climate relations. Across a 30-year time series, the $\delta^{13}C$ and $\delta^{18}O$ values of the earlywood (EW) cellulose in the annual rings of *Pinus ponderosa* reflected relatively high intrinsic water-use efficiencies and high evaporative fractionation of $^{18}O/^{16}O$, respectively, compared with the false latewood (FLW), summerwood (SW), and latewood (LW) subdivisions. This result is counterintuitive, given the spring origins of the EW source water and midsummer origins of the FLW, SW, and LW. With the use of the Craig–Gordon (CG), isotope-climate model revealed that the isotope ratios in all of the ring subdivision are explained by the existence of seasonal lags, lasting several weeks, between the initial formation of tracheids and the production of cellulosic secondary cell walls during maturation. In contrast to some past studies, modification of the CG model according to conventional methods to account for mixing of needle water between fractionated and nonfractionated sources did not improve the accuracy of predictions. Our results reveal new potential in the use of tree-ring isotopes to reconstruct past intra-annual tree–climate relations if lags in cambial phenology are reconciled with isotope ratio observations and included in theoretical treatments.

KEYWORDS

arid, dendroclimatology, drought, humidity, monsoon, montane, pine, precipitation, snowpack, xylogenesis

1 | INTRODUCTION

Stable isotope ratios of carbon ($\delta^{13}C$) and oxygen ($\delta^{18}O$) measured in tree-ring cellulose are commonly used as indicators of the ecophysiological processes and associated climate conditions that govern tree growth (McCarroll & Loader, 2004). The $\delta^{13}C$ of photosynthetically assimilated CO_2 is determined by kinetic fractionations associated with the diffusive pathways of the leaf and the biochemical discrimination associated with the active sites of Rubisco enzymes in chloroplasts (Farquhar, Hubick, Condon, & Richards, 1989a). The dependence of photosynthetic carbon isotope fractionation ($\Delta^{13}C$) on the ratio of leaf intercellular and ambient CO_2 concentrations (c_i/c_a) provides a reliable proxy for intrinsic water-use efficiency (iWUE; Farquhar et al., 1989a) and has been used in tree-ring studies to characterize past environmental effects on the coupling between leaf–atmosphere carbon and water exchanges (Frank et al., 2015; Leavitt, 1993; Saurer et al., 2014). The oxygen isotope composition of CO_2 is influenced by the enzyme-catalyzed interconversion of CO_2 and HCO_3^- in the leaf water pool during photosynthetic CO_2 assimilation. The CO_2—HCO_3^- interconversion allows photoassimilated CO_2 to record the isotopic signal of leaf water, which, in turn, is determined by the combined influences of the $\delta^{18}O$ of precipitation, atmospheric vapor pressure deficit (VPD), kinetic and equilibrium evaporative exchanges between the leaf and

atmosphere, and the mixing of nonfractionated (xylem) and fractionated (mesophyll) water in the leaf (Barbour, Roden, Farquhar, & Ehleringer, 2004; Dongmann, Nurnberg, Forstel, & Wagener, 1974; Farquhar & Lloyd, 1993). Recognition of the connections among the $\delta^{18}O$ of cellulose, precipitation $\delta^{18}O$, and atmospheric VPD has provided the foundation for the reconstruction of past hydroclimate regimes and associated tree responses (Barbour, Walcroft, & Farquhar, 2002; Roden & Ehleringer, 1999; Roden, Johnstone, & Dawson, 2009; Szejner et al., 2016; Wright & Leavitt, 2006a).

The theoretical underpinnings of the proximal processes coupling carbon and water exchanges between the leaf and atmosphere, and their control over the isotopic composition of photosynthate in the leaf, have been well-defined (Cernusak et al., 2016). However, there are several steps after photosynthetic CO_2 assimilation with the potential to alter the isotope composition of tree-ring cellulose (Gessler et al., 2013). In one of the most important, a fraction of the carbonyl oxygens in phloem-transported sucrose exchanges with the oxygens of nonfractionated xylem water during cellulose synthesis (Farquhar, Barbour, & Henry, 1998; Sternberg, Pinzon, Anderson, & Jahren, 2006). These secondary steps have been poorly represented in past theoretical treatments of tree-ring isotope fractionation, and the lack of process-based insight has impeded our ability to partition the influences of climate on the ultimate oxygen isotope ratio of tree-ring cellulose, and to precisely align tree-ring carbon and oxygen isotope signals with intra-annual (seasonal) climate dynamics (Gessler et al., 2009, 2014).

Tree-ring formation (xylogenesis) is a dynamic process (Rossi, Morin, & Deslauriers, 2012) that can vary seasonally, and among tree functional types (e.g., needle-leaved and broad-leaved trees) and species (Lachenbruch & McCulloh, 2014). Xylogenesis has two main sequential cellular processes (Rathgeber, Cuny, & Fonti, 2016): enlargement of the xylem cells (radial growth of the primary cell wall) and cell wall thickening (radial growth of the secondary cell wall). The development of the primary cell wall entails relatively small quantities of cellulose production (Cuny et al., 2015), meaning that most of the cellulosic signal from which to reconstruct isotope–climate relations comes from the cell wall thickening phase. An understanding of the timing and pace of this phase is critical to correctly interpret stable isotope ratios in the tree-ring record (Cuny et al., 2015; Cuny & Rathgeber, 2016; Ogée et al., 2009). Variations in the timing and duration of the cell enlargement and cell wall thickening phases as the tree ring develops varies in response to seasonal climate gradients and is reflected in anatomically distinct tree-ring cell types. In conifers, these cell types include earlywood (EW), which consists of large, thin-walled cells, and latewood (LW), which consists of narrow, thick-walled cells. Generally, EW is formed at the beginning of the growing season and LW at the end. In conifers from semiarid sites, it is not uncommon to observe a narrow band of LW-like cells within the EW portion of the tree ring (Battipaglia et al., 2016). These narrow bands are often referred to as intra-annual density fluctuations, or false LW (FLW), a term that we will use here to invoke analogies to the EW and LW regions of annual rings. The production of FLW is associated with the slowing down or cessation of cambial activity following stomatal closure in response to midseason drought stress (Battipaglia et al., 2014; Campelo, Gutiérrez, Ribas, Nabais, & Freitas, 2007; De Micco et al., 2016; Pflug et al., 2015; Sarris, Siegwolf, & Körner, 2013). The production of FLW is often followed by a band of EW-like cells, which immediately precede the LW; this post-FLW band of cells is referred to here as summerwood (SW). The serial combination of EW, FLW, SW, and LW provides a means of studying the seasonal progression of isotope–climate relations, an approach which has been exploited in some past studies (Barbour et al., 2002; Helle & Schlesser, 2004; Leavitt et al., 2011; Roden & Ehleringer, 2007; Szejner et al., 2016), though typically with regard to only EW and LW.

Recent insights into xylogenesis have improved our ability to align specific phases of ring formation and climate drivers for isotope analysis, while at the same time calling into question the interpretations of past seasonal studies of tree-ring isotopes. For instance, Cuny et al. (2013) found that in pine trees in France, EW cells formed early in the growing season may spend up to 20 days in the enlargement phase before passing into the cell wall thickening phase. This means that the climate drivers reflected in the isotope ratios of EW cellulose would be lagged by at least 3 weeks from the onset of cell formation. In the same study, pine LW cells were found to spend only about 5 days in the enlargement phase but up to 50 days in the cell wall thickening phase. Once again, this introduces seasonal lags in cambial phenology into analyses of tree-ring attributes. For LW cells, the potential for error exists if the alignment of climate drivers and isotope analysis is based on the timing for the onset of cell formation, without consideration of the longer late season time-span that underlies secondary cell wall formation. Environmental and physiological tree-ring-based studies would benefit from systematic investigations at intra-annual time-scale to integrate the kinetics of xylogenesis with the theoretical understanding of isotope–climate relations (Vaganov, Anchukaitis, & Evans, 2011; Wright & Leavitt, 2006a).

In the present study, we examined the carbon and oxygen isotope ratios in EW, FLW, SW, and LW in ponderosa pine (*Pinus ponderosa*), a ubiquitous tree species of semiarid, montane forests in the western United States (Graham & Jain, 2005). The climate in the southwestern range of *P. ponderosa* is characterized by a bimodal distribution of precipitation (Figure 1; Sheppard, Comrie, Packin, Angersbach, & Hughes, 2002), with a winter season dominated by frontal storms and a summer season marked by convective storms related to the North American monsoon system (Adams & Comrie, 1997; Higgins, Yao, & Wang, 1997). In past ring-width studies, researchers have found that the formation of EW is associated with the early season snowmelt period and LW is associated with the mid-to-late summer monsoon period (Griffin et al., 2013; Meko & Baisan, 2001). The early and late season precipitation pulses in the southwestern United States are separated by a hyperarid period, typically in June (Figure 1), during which soil and air moisture contents are extremely low (Budelsky, 1969; Wright & Leavitt, 2006b). Observations of ponderosa pine in southern Arizona have shown that the pace of the cell wall development phase slows down in the face of seasonal water stress during the hyperarid period, prior to the arrival of monsoon storms (Budelsky, 1969; Fritts, 1976; Fritts, Vaganov, Sviderskaya, & Shashkin, 1991; Vaganov, Hughes, & Shashkin,

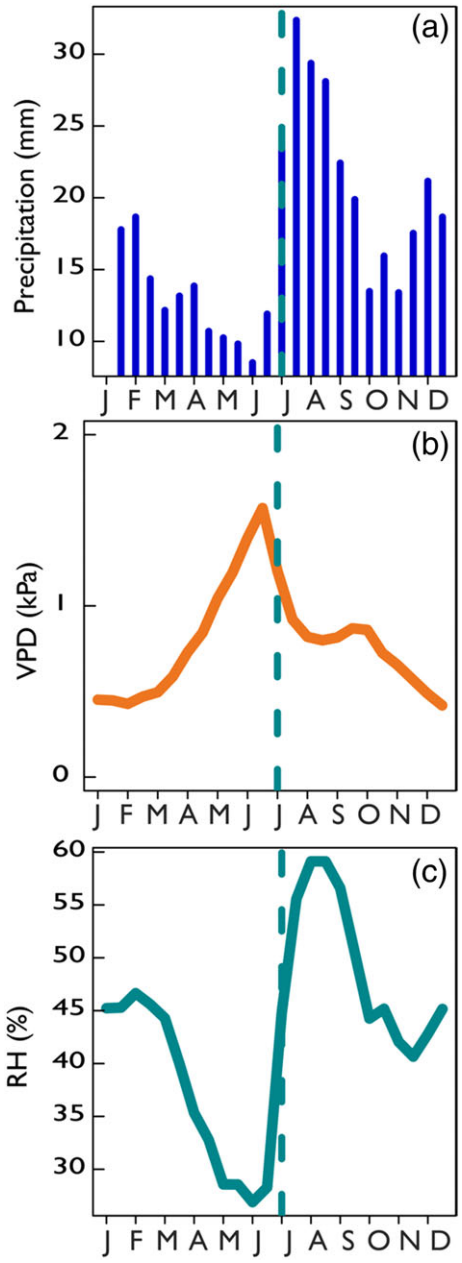

FIGURE 1 (a) Monthly total precipitation in millimeter, (b) vapor pressure deficit (VPD) in kilopascal, and (c) relative humidity (RH) in percent for the study site located in the Santa Catalina mountains (Arizona). The data are averaged from 1985 to 2015. The dashed turquoise line indicates the onset of the monsoon season: ~July 7 ± 10 days. Climate data were derived from PRISM (Daly et al., 2008)

2006). It is at the end of this slow growth phase that FLW cells are initiated.

Our aims in this study were to (a) combine xylogenesis observations of the different phases of tree-ring formation with isotopic analyses of serial sections through the rings in order to define seasonal lags in the isotope–climate relation and properly align isotope fractionation processes with associated climate drivers; (b) use aligned isotope–climate relations to understand the seasonal hydroclimate (precipitation vs. atmospheric humidity) controls on isotope fractionation; and (c) test existing models of isotope fractionation in tree rings against 30 years of reconstructed isotope–climate relations in a site with distinct winter and summer precipitation regimes separated by a hyperarid late spring period.

2 | MATERIALS AND METHODS

2.1 | Study site and species

The study site is in the Santa Catalina Mountains, near Tucson, Arizona, USA, at an elevation of ~2,200 m. The site was selected for having trees between 70 and 100 years old, which frequently exhibit FLW bands (Babst et al., 2016; Wright, 2001). Two cores (12-mm diameter) were taken from 20 trees, and ring-width chronologies were developed using standard dendrochronological techniques (Stokes & Smiley, 1996). A subset of three trees exhibiting FLW bands in almost every year (Figure 2) were then selected for analyses of $\delta^{18}O$ and $\delta^{13}C$ for the 30-year period 1985–2014.

The timing of cell development for EW, FLW, SW, and LW subdivisions is shown in Figure 2b. These early xylogenesis observations of histological samples (Budelsky, 1969) show only the timing of cell initiation and maturity without indicating the duration of the cell size enlargement and cell wall thickening phases. They provide, however, the range of dates during which the cells of each tree-ring subdivision became mature (Figure 2b); therefore, the period and associated climate conditions under which isotope signals are integrated in the cellulose. For instance, the $\delta^{18}O_{cel}$ of the FLW, initiated in June and matured by the end of July, is expected to integrate climate conditions from both the hyperarid period in June and the summer monsoon in July. Recognizing that nearly five decades have passed since publication of the detailed cambial analysis by Budelsky (1969), we checked the timing of the various phases of xylogenesis in trees from this site with observations in 2014. We obtained observations on the seasonal progression of xylogenesis (Table S3; Morino and Hughes, University of Arizona, in preparation) to estimate lags between cell enlargement and cell wall thickening phases, and the duration of cell wall thickening phase. The more recent values, reported in Table S3, were used to determine xylogenesis lags in the modeling of seasonal isotope ratios.

Microcores (2-mm diameter) were collected on a weekly basis from the north side of trees using a Trephor extraction tool (Rossi, Anfodillo, & Deslauriers, 2006) and placed in a 50% ethanol solution at 5°C (Deslauriers, Rossi, Anfodillo, & Saracino, 2008). Samples were dehydrated by immersion in successively concentrated solutions of ethanol, then finally in D-limonene (Rossi et al., 2006). After being embedded in paraffin, thin sections (6–8 microns) were cut with a rotary microtome, stained with cresyl fast violet, and observed at 200× to 400× magnification. The phases of tracheid differentiation were distinguished by cell shape, size, color, and birefringence and scored according to the phenological phases used in the determination of cellulose isotope ratios. For each sample, three cell files were selected and the number of cells in each phase were scored and averaged. Cell counts in each phase were normalized to consider differences in radial growth rates around the circumference of the tree (Rossi, Deslauriers, & Morin, 2003) and then smoothed to further enhance the signal-to-noise ratio (Cuny et al., 2013).

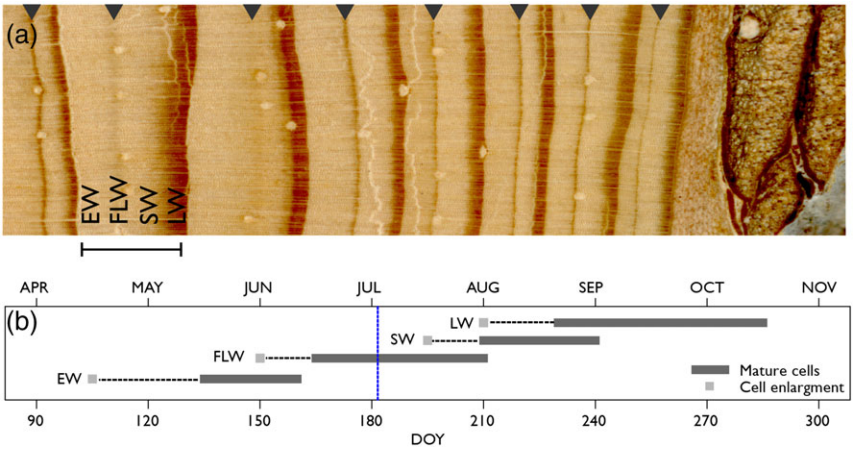

FIGURE 2 (a) Photograph of tree rings from a ponderosa pine growing in the Santa Catalina mountains. Each ring contains a false latewood band (FLW) indicated by black triangles. The typical anatomical subdivisions of an annual ring (indicated by a horizontal bar) are shown and labelled as follow: Earlywood (EW) located before the FLW, summer wood (SW), and latewood (LW) both located after the FLW; (b) cell wall enlargement and thickening at maturity observed from March to October 1966 in a *Pinus ponderosa* growing in the same mountains range (Budelsky, 1969). The x-axis at the bottom indicates the day of the year (DOY), and the x-axis at the top indicates the corresponding months. The gray squares indicate the onset of the first cell enlargement for each tree-ring subdivision. The dark gray bars indicate the range of dates when the first and last cells of each subdivision finished thickening and became mature cells. For instance, the first EW cell started enlarging in mid-April (DOY 105) and was mature by mid-May (DOY 135), whereas the last EW cell was mature by early June (DOY 165). The vertical blue dashed-line indicates the date of the monsoon onset [Colour figure can be viewed at wileyonlinelibrary.com]

For isotopic analyses, growth rings were subdivided into five consecutive sections, based on observations of anatomical features related to cell size (Supporting Information): two equal-width sections before the FLW, called earlywood 1 (EW1) and earlywood 2 (EW2); one section of FLW; one SW section after the FLW; and one LW section. Two exceptions to this sampling design were (a) years where the FLW position was relatively close to the previous ring boundary (n = 5), in which case, we only distinguished one EW section and (b) years where the FLW position was close to the LW (n = 5) in which case no SW was used. For years without an FLW (n = 3), the ring was either separated individually or divided into two or three equal parts, depending on the EW bandwidth.

Wood samples were ground to 20 meshes, and α-cellulose was extracted from each ground sample following Green (1963), as modified by Leavitt (1993) and with the addition of a NaOH extraction step to remove hemicelluloses, followed by sonication to ensure homogeneity (Laumer et al., 2009). Cellulose samples were analyzed for carbon and oxygen isotope ratios ($\delta^{13}C_{cel}$ and $\delta^{18}O_{cel}$, respectively) using isotope–ratio mass spectrometry at the University of Maryland, following the protocol described in Evans, Selmer, Breeden, Lopatka, and Plummer (2016). The overall precision values for the corrected data, based on replicate standard analyses, are 0.10‰ for $\delta^{13}C$ and 0.25‰ for $\delta^{18}O$. The $\delta^{13}C_{cel}$ values were corrected for the decline of atmospheric $^{13}C/^{12}C$ ratio since the industrial revolution following the procedure described in McCarroll et al. (2009) and using Northern Hemisphere atmospheric CO_2 concentrations and atmospheric $\delta^{13}C$ ratios available from the Mauna Loa observatory in Hawaii (Keeling et al., 2005).

2.2 | Mechanistic modeling of tree-ring cellulose $\delta^{18}O_{cel}$

Modeling that aims to couple $\delta^{18}O_{cel}$ to the surrounding environment begins with consideration of leaf water, which has the potential to exchange oxygen isotopes with CO_2 during photosynthesis. The $\delta^{18}O$ of leaf water reflects the combined influences of the $\delta^{18}O$ of source water modified by kinetic and equilibrium fractionations between the leaf and atmosphere during transpiration (Barbour et al., 2004; Dongmann et al., 1974; Farquhar & Lloyd, 1993). Modeling of this dynamic interaction starts from the Craig–Gordon model (Craig & Gordon, 1965; Dongmann et al., 1974) which assumes water vapor saturation for air inside the leaf:

$$\Delta_e \approx \varepsilon^+ + \varepsilon_k + (\Delta_v - \varepsilon_k)\frac{w_a}{w_i}, \quad (1)$$

where Δ_e is the isotopic discrimination (fractionation; Farquhar, Hubick, Condon, & Richards, 1989b) or isotopic enrichment of water at the evaporative sites inside the leaf, compared with the source water (Barbour et al., 2004; Cernusak et al., 2016; Farquhar & Lloyd, 1993); ε^+ and ε_k are the equilibrium (associated with phase transition) and kinetic fractionations, respectively (Majoube, 1970). Δ_v is isotopic enrichment of vapor relative to source water, w_a is the mole fraction of water vapor in the ambient air (assuming a negligible leaf boundary layer), and w_i is the mole fraction of water vapor in the leaf. The observed overall enrichment of evaporating leaf water is seldom as great as that predicted by Equation (1). Recognition of this discrepancy has led to modification of the model in one of two ways: (a) a

transport-based kinetic dilution of Δ_e through mixing of enriched and nonenriched water in the leaf (the Péclet effect; Farquhar & Cernusak, 2005; Farquhar & Lloyd, 1993) and (b) a simpler, linear mixing of two pools of leaf water (Roden, Kahmen, Buchmann, & Siegwolf, 2015; Song, Loucos, Simonin, Farquhar, & Barbour, 2015), one enriched (mesophyll) and one not (xylem):

$$\Delta_L = \Delta_e(1-e^{-\wp})/\wp(\text{Peclet modification}), \quad (2)$$

$$\delta_{L=}\delta_e\ (1-f_u) + \delta_{wx}f_u\ (\text{Two-pool modification}), \quad (3)$$

In Equation (2), $\wp$ is the Péclet number and reflects the ratio between advective and diffusive transport of liquid water in the leaf (Farquhar & Lloyd, 1993):

$$\wp = \frac{EL}{CD}, \quad (4)$$

where E is the transpiration rate (mol·m^{-2}·s), L is the effective path length (m) for the advective flow in the leaf and describes the distance and tortuosity of the water flow pathway, C is the molar density of water (55.5 × 10^3 mol/m^3), and D is the diffusivity of $H_2{}^{18}O$ in water (m^2/s). Equation (2) describes the gradient in $H_2{}^{18}O$ enrichment in leaf water due to the advective flow of source water from the xylem toward the sites of transpiration opposed by the backward diffusion of evaporatively enriched water from the evaporative sites. Accordingly, as E increases, we expect less enrichment of the heavier isotopes in the total leaf water pool. Equations (2) and (4) require a critical constraint on the effective path length (L) that is difficult to estimate accurately and varies among species (Kahmen et al., 2008; Roden et al., 2015; Song, Barbour, Farquhar, Vann, & Helliker, 2013). In Equation (3), the notation has switched from enrichment (Δ) to delta-notation (δ) and includes the isotope ratio of the nonenriched xylem water pool (δ_{wx}) and the fraction of leaf water in that pool not subject to evaporative enrichment (f_u; Roden et al., 2015; Song et al., 2015). Conifer needles are difficult for predicting Péclet modifications (Equations (2) and (4)) due to uncertainties in transport path length, velocity of water movement and the degree of suberization of new needle xylem (Roden et al., 2015; Song et al., 2013). The simpler two-pool model may be more appropriate (Roden et al., 2015).

Photosynthate that reflects the isotopic fractionation of needle water is potentially fractionated further during cellulose synthesis. A fraction of the carbonyl oxygens in phloem-transported sucrose can potentially exchange with the oxygens of nonenriched xylem water during cellulose synthesis (Sternberg et al., 2006). This secondary fractionation of cellulose oxygen (Δ_c) can be defined as follows:

$$\Delta_c = \Delta_L(1-P_{ex}P_x) + \varepsilon_{wc}, \quad (5)$$

where P_x is the fraction of cambial cellular water that is not isotopically enriched ($P_x \approx 1.0$), and P_{ex} is the fraction of carbonyl oxygen atoms that exchange with nonenriched water. Typically, a value of 0.20–0.42 is used for P_{ex} for $^{18}O/^{16}O$ (Cernusak, Farquhar, & Pate, 2005; Helliker & Ehleringer, 2002; Roden & Ehleringer, 2000; Sternberg & Ellsworth, 2011), but these values are from greenhouse experiments and little is known about how P_{ex} varies in situ seasonally or across spatial gradients. ε_{wc} is the equilibrium fractionation factor (ε_{wc} = 27‰) between carbonyl oxygen and water (Sternberg, Deniro, & Savidge, 1986).

2.3 | Model parameterization

We used the three mechanistic models described above (unmodified CG [Equation (1)], C-G modified for Péclet effect [CG-PM, Equation (2)], and C-G modified for two-pool mixing [CG-2P, Equation (3)]) to simulate isotopic enrichment of evaporative site water (Δ_e) and bulk leaf water enrichment or isotope ratio (Δ_L and δ_L, respectively) as functions of the atmospheric vapor pressure deficit (VPD) and $\delta^{18}O$ composition of source water. All three models assume isotopic steady-state conditions, that is, the isotopic composition of transpired water vapor is identical to source water (Craig & Gordon, 1965; Farquhar & Cernusak, 2005; Farquhar, Cernusak, & Barnes, 2007). In parameterizing the three models, we made the following assumptions and step calculations:

[1] Needle temperature is equal to air temperature.

[2] Source water (xylem) is determined as a 6-week moving average of weighted mean $\delta^{18}O$ determined from precipitation samples (Figure 3a,b), which were collected 1 km from the study site at the same elevation (Wright, 2001). This procedure smoothly integrates individual precipitation events into the source-water isotope composition and provides a lagged influence of precipitation events on the source (i.e., provides a soil residence interval to precipitation sources).

[3] Stomatal conductance g_s (mmol·m^{-2}·s^{-1}) depends on atmospheric VPD in kPa and is calculated using observations on ponderosa pine from a semiarid environment (McDowell, White, & Pockman, 2008), similar to that of the study site used here:

$$g_s = 283.2e^{(-1.15VPD)}. \quad (6)$$

[4] Transpiration rate E (mol·m^{-2}·s^{-1}) is estimated using the following:

$$E = (w_i - w_a)g, \quad (7)$$

where w is the vapor pressure mole fraction of water vapor and the subscripts i and a are intercellular air spaces and ambient air, respectively, and g (mmol·m^{-2}·s^{-1}) is the total leaf conductance to water vapor. Values for w_a and w_i were determined from daily humidity and air temperature estimates obtained for the site as described below in Section 2.4.2.

[5] The Péclet number (dimensionless) is numerically resolved using E estimates (Equation (3)) and the following:

[5.1]. D (m-^{2}/s) which is dependent on temperature in Celsius (Cuntz, Ogee, Farquhar, Peylin, & Cernusak, 2007):

$$D = 119X10^{-9}e^{\left(\frac{-637}{136.15+T}\right)}. \quad (8)$$

[5.2]. The effective path length L (m) which is calculated using an inverse relationship between E (mol·m^{-2}·s^{-1}) and L (Song et al., 2013):

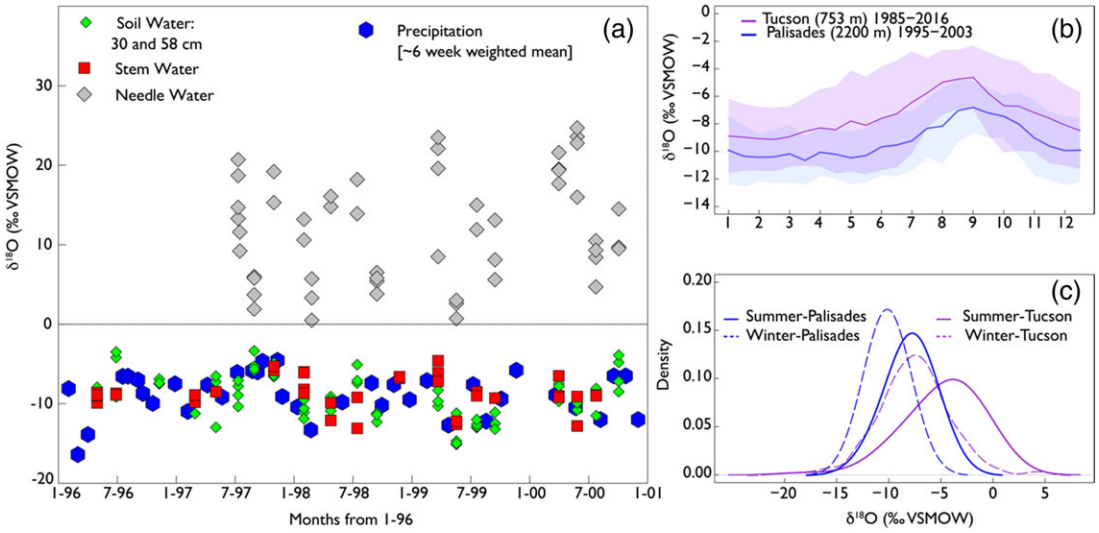

FIGURE 3 (a) Seasonal variations in soil (30 and 58 cm depth), xylem, and needle water $\delta^{18}O$. Samples were collected from the Santa Catalina site between 1995 and 2001. A 6-week weighed mean of precipitation $\delta^{18}O$ is plotted in blue diamonds and indicates that precipitation events are well mixed into deep soil water pools and are similar to xylem $\delta^{18}O$; (b) annual pattern of precipitation $\delta^{18}O$ from Palisades (PRS, 1 km from study site) in blue and from Tucson–University of Arizona in magenta with their respective standard deviations in shaded colors. The $\delta^{18}O$ corresponds to a 6-week weighed mean; (c) Seasonal distribution of winter (solid) and summer (dashed) $\delta^{18}O$ of precipitation from Tucson–University of Arizona site between 1985 and 2016 in magenta color and from PRS between 1995 and 2003 in blue color [Colour figure can be viewed at wileyonlinelibrary.com]

$$L = 2.33X10^{5}E^{-1.20}. \quad (9)$$

In a first step, we used the three mechanistic models to predict the needle evaporative enrichment and compared it to isotopic measurements of needle water available at the study site from 1997 to 2000. This step allowed us to evaluate which of the three models best predicted the observed needle water enrichment. In a second step, the model with the best predictive accuracy was used to predict the Δ_L of needle water and $\delta^{18}O$ cellulose ($\delta^{18}O_{cel}$) from 1985 to 2014. For these two steps, we made the following assumptions:

[6] For the CG-2P model, we varied the proportion of the bulk needle tissue that is not subjected to evaporative enrichment of ^{18}O, f_u, from 0.1 (bulk leaf water dominated by enriched water) to 0.9 (bulk leaf water not enriched).

[7] For $\delta^{18}O_{cel}$ simulations, we conducted a sensitivity analysis and varied P_{ex} (the proportion of exchangeable oxygen in cellulose) values within the range most frequently reported in the literature (0.1–0.8) by increments of 0.1.

2.4 | Site level conditions and input data

2.4.1 | Isotopic data

Isotopic data used to simulate needle Δ_L and δ_L to test the CG, CG-PM, and CG-2P were taken from previously published work using trees from the same site (Figure 3; Wright, 2001). In brief, needles and stem water were collected from the study site every 3 months during four growing seasons from 1997 to 2000. We used the $\delta^{18}O$ of stem water as source water to simulate the isotopic enrichment in atmospheric water vapor, relative to source water (Δ_v), and the $\delta^{18}O$ of needle water to calculate the isotopic enrichment of bulk leaf water (Δ_e), above the source water.

Isotopic data used to simulate $\delta^{18}O_{cel}$ from 1985 to 2014 were based on 8 years of precipitation $\delta^{18}O$ ($\delta^{18}O_{PCP}$) collected between 1995 and 2003, at a climate station located 1 km from the study site at roughly biweekly resolution. From this, we produced 6-week weighted composites which were averaged to estimate the local annual pattern of $\delta^{18}O_{PCP}$ (Figure 3b). This annual pattern is consistent with $\delta^{18}O_{PCP}$ obtained from measurements nearby, at the University of Arizona (753-m elevation), between 1981 and present (Eastoe & Dettman, 2016), although ~2‰ more enriched than at our study site (Figures 3b-c and S3). Precipitation in the study area is characterized by two wet seasons: (a) a winter season extending from October to April in which moisture originates mostly from the northern Pacific Ocean and (b) a summer monsoon season extending from July to September in which moisture originates mostly from the Gulf of California and the Gulf of Mexico (Hu & Dominguez, 2014). This bimodal precipitation regime is also expressed in the $\delta^{18}O_{PCP}$ (Figure 3c) with weighted average $\delta^{18}O_{PCP}$ of −10.15 ± 0.15‰ for winter and −7.94 ± 1.69‰ for summer.

2.4.2 | Meteorological data

For meteorological data, mean, maximum, and minimum T_{air} and T_{dew} were obtained for 1981–2015 at daily resolution, from the Parameter-elevation Relationships on Independent Slopes Model (PRISM) dataset at 4-km resolution (Daly et al., 2008) using the interpolation option in the online data explorer to take into account values from surrounding grid cells (http://www.prism.oregonstate.edu/explorer/, 04/26/2017; Figure S1). The data were extracted using the study site's coordinates and elevation at an elevation of 2,150 m. For

simulations of leaf Δ_L and δ_L from 1997 to 2000, mean daily values of T_{air} and T_{dew} for sampling days were used to calculate VPD between the actual vapor pressure and the saturated vapor (VPD) and relative humidity (RH). For simulations of $\Delta_L$and $\delta^{18}O_{cel}$ from 1985 to 2014, biweekly (15 days) aggregates were computed from daily data of T_{air} and T_{dew} to calculate VPD and RH (Figure S1).

3 | RESULTS

3.1 | Tree-ring seasonal isotope signal

The cellulose $\delta^{13}C$ and $\delta^{18}O$ values were significantly coherent among all trees and across the 30-year time series, with mean interseries correlations of 0.67 for $\delta^{13}C_{cel}$ and 0.8 for $\delta\ ^{18}O_{cel}$ ($P < 0.001$; Table S1). Values of cellulose $\delta^{13}C$ and $\delta^{18}O$ displayed a distinct seasonal pattern (Figure 4). For $\delta^{13}C_{cel}$ (Figure 4a), the mean value at the beginning of the annual rings, in the earliest EW (EW1), was −21.76 ± 0.6‰, which increased to −21.28 ± 0.5‰ at the later EW subdivision (EW2). At the FLW subdivision, mean $\delta^{13}C_{cel}$ values decreased to −21.50 ± 0.4‰ and progressed to an even lower value of −22.01 ± 0.4‰ for the SW subdivision. Similar low values were observed for the LW subdivision with a mean value of −21.98 ± 0.4 ‰, marking the end of the seasonal pattern. For $\delta\ ^{18}O_{cel}$ (Figure 4b), the highest values were observed for EW1 with 36 ± 1.3‰, followed by a decline in subsequent subdivisions. EW2 had a mean value of 34.63 ± 1.3‰ and the FLW and SW subdivisions had the lowest values of 32.56 ± 0.9‰ and 32.28 ± 0.9‰, respectively. The end of the seasonal pattern was marked by an increase of the $\delta\ ^{18}O_{cel}$ in the LW subdivision with a mean value of 33.81 ± 1.04‰. The seasonal subdivision mean isotopic values were statistically different ($P < 0.001$); more so for $\delta\ ^{18}O_{cel}$ than $\delta^{13}C_{cel}$ (Table S2).

3.2 | Model-data comparisons and model intercomparisons

3.2.1 | Leaf water enrichment (Δ_L)

Simulations of leaf water enrichment Δ_e and leaf water δ_L using the CG, CG-PM, and CG-2P models from 1997 to 2000 are shown in Figure 5, plotted against the measured Δ_e and δ_L values. The unmodified CG model explained 77% of the variance in Δ_L (Figure 5 a), though it overestimated Δ_L for some needles during the high-humidity season (July to September) and exhibited an overall slope of less than one (0.92, $P < 0.001$), lying above the 1:1 line. The CG-PM model explained 72% of the variance in Δ_L (Figure 5b), and it substantially underestimated Δ_L across all seasons with a slope significantly different from unity (0.61, $P < 0.001$), lying below the 1:1 line. The CG-2P model results explained 75% of the variance in δ_L when a 0.1 fraction (f_u) of needle water was specified as not subject to evaporative enrichment (Figure 5c). The CG-2P model underestimated the δ_L with a slope of less than one (0.88, $P < 0.001$), lying below the 1:1 line. The modeled versus measured δ_L slope further departed from the 1:1 line when the proportion of f_u was specified as higher (0.2 and 0.3). Overall, the leaf water ^{18}O enrichment modeling demonstrated that the unmodified CG model provided the most accurate predictions of the observed data, with data from all seasons falling closest to the 1:1 line.

The predictive accuracy of the three models can be additionally evaluated by investigating the fractional difference between predicted and observed bulk leaf water enrichment at the evaporation sites ($f = 1\text{-}\Delta_L/\Delta_e$; Barbour et al., 2004; Cernusak et al., 2016). Analysis of f confirms that the unmodified CG model overestimated ^{18}O enrichment, although marginally, with an average proportional difference of 0.04. If it exists, a positive relationship between f and transpiration (E) should reflect the Péclet effect (Barbour, Schurr, Henry, Wong, & Farquhar, 2000); however, we found no relationship between estimated E and f (results not shown). These results are in line with the conclusions of a recent synthesis by Cernusak et al. (2016).

Estimated values of E for trees at our site during the growing season were low (1.0–1.2 $mmol{\cdot}m^{-2}{\cdot}s^{-1}$). Using the empirical relationship (Equation (9)) of Song et al. (2013), the estimated mean L was 78 mm (Figure S2). The values of L for *P. ponderosa* at our site appear to be considerably larger than those required for an accurate prediction of leaf water enrichment, as the CG-PM model substantially underestimated the value of Δ_L ($f = -0.4$), particularly for low humidity seasons. The large value of L would cause a decrease in the influence of evaporative enrichment on the average Δ_L, by impeding the diffusion of enriched ^{18}O away from evaporative sites.

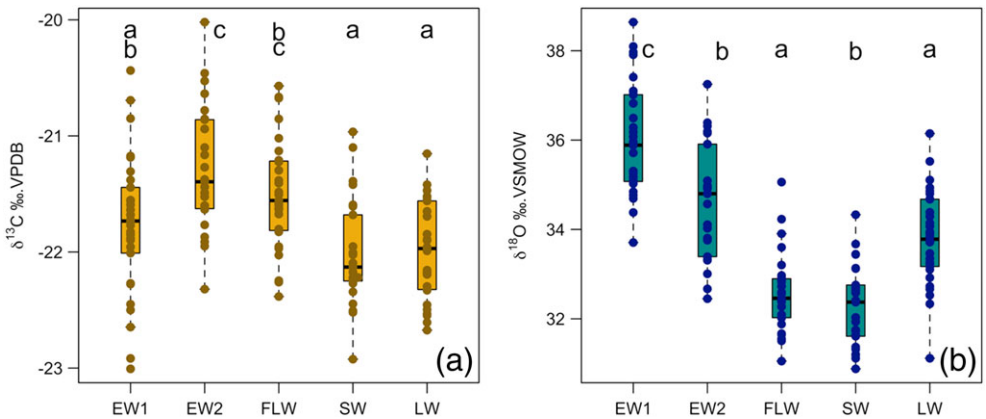

FIGURE 4 Tree-ring seasonal isotope signal. Box and whiskers plots of cellulose values from 1985 to 2014 of (a) $\delta^{13}C_{cel}$ and (b) $\delta^{18}O_{cel}$ averaged from three trees at each ring subdivision (EW1, EW2, FLW, SW, and FLW). The letters at the top of each panel indicate the statistical significance between the mean isotopic values of each tree-ring subdivision. Boxes sharing the same letters are not significantly different based on Tukey Honest Significant Differences (HSD) test [Colour figure can be viewed at wileyonlinelibrary.com]

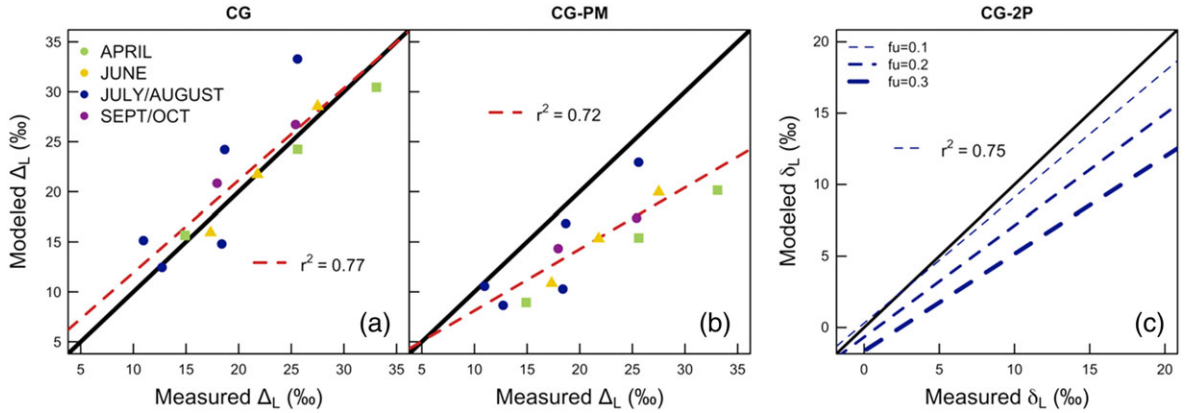

FIGURE 5 Mechanistic modelling of the leaf water enrichment above the source Δ_L [Left and Center Panels] and leaf water δ_L (Right panel) for the period from 1997 to 2000. (a) The unmodified Craig–Gordon model (CG), (b) the Péclet effect modified model (CG-PM) using a negative relationship between transpiration rate (*E*) and effective path-length (*L*), (c) the Craig–Gordon 2-pool model (CG-2P). Solid lines represent 1:1 relationships, and dashed lines represent a least square regression between measured and modelled Δ_L values (Panels a and b) and δ_L values (Panel c). The colored symbols in panels a and b represent the seasons of needle sampling. The multiple dashed lines in panel c represent different values of the fraction of the needles tissues that is not subjected to enrichment (f_u) [Colour figure can be viewed at wileyonlinelibrary.com]

The negative relationship between *L* and *E* (Equation (9)) that we observed at low values of *E* (<1.5 mmol·m^{-2}·s^{-1}) might be due to covariance between *E* and *L* in response to increasing VPD, which may be controlled by symplastic water fluxes (Song et al., 2013). However, the covariance could also have resulted from nonsteady-state conditions (Cernusak & Kahmen, 2013; Loucos, Simonin, Song, & Barbour, 2015) which will cause an overestimation of *L*, especially when applied to species with low-transpiration rates and low stomatal conductance (Cernusak et al., 2005; Offermann et al., 2011), such as for *P. ponderosa* (Budelsky, 1969).

With use of the CG-2P model, we were forced to parameterize f_u as a relatively low value of 0.1, to generate predictions of δ_L that approximated observations (Figure 5c). A sensitivity analysis of the influence of f_u on error between observed and predicted δ_L values when f_u = 0.1 revealed that the CG-2P model underestimated δ_L (f = −0.23). The best fit between observed and modeled δ_L values for the high humidity season was obtained with a fraction of f_u = 0.2. The derived estimates of f_u of 0.2 are within the range reported for conifer new needles 0.2 ± 0.01 (Roden et al., 2015). In our needles, however, there is no unique value for f_u that accurately predicts δ_L in both high and low humidity seasons.

3.2.2 | Tree-ring cellulose $\delta^{18}O$ ($\delta^{18}O_{cel}$)

After evaluating the predictive accuracy for all three models, we concluded that the CG model was most adequate for further analysis. This is in line with earlier findings by Roden and Ehleringer (2000) that the CG model accurately described the leaf water enrichment in a wide range of environments.

Results of the $\delta^{18}O_{cel}$ using the CG model are shown in Figure 6. The CG model adequately captured the observed seasonal pattern of the $\delta^{18}O_{cel}$ cycle (Figure 6a). However, the results indicate the necessity to invoke a time lag between cell enlargement (cell size and radial growth) and cell wall thickening (isotopic composition of cellulose). We determined values for seasonal lags from microscopic analysis of microcore samples collected weekly during 2014 (Morino and Hughes, University of Arizona, unpublished data). These lags correspond to the onset and duration of the cell wall thickening phase and were between 2 and 10 weeks, depending on which anatomical subdivision was being considered (Tables 1 and S3). Average climate conditions for successive 2-week intervals during the thickening phase were used as inputs for the model of $\Delta^{18}O$ of cellulose. The model output was also determined at biweekly resolution. The model output was then averaged over the period of observed cell wall thickening for each tree-ring subdivision and compared with the bulked and observed $\Delta^{18}O_{cel}$ value for that subdivision. These procedures include the assumptions that for each subdivision: (a) that the observed isotope ratios for each tree-ring subdivision reflect integration of climate conditions across the observed phase of cell wall thickening and (b) at a constant rate of cellulose deposition (Figure 6a). Agreement between observed and modelled $\delta^{18}O_{cel}$ values was assessed using estimates of root mean square error (Table 1).

The modeled $\delta^{18}O_{cel}$ values indicate that the early growing season is characterized by high $\delta^{18}O_{cel}$, which reaches a peak in mid-June, followed by a decline during the monsoon season (July and August). The end of the growing season (September and October) is marked by an increase in modeled $\delta^{18}O_{cel}$ values. The $\delta^{18}O_{cel}$ simulations were run for a range of exchangeable oxygen fractions (between sucrose and H_2O; P_{ex}), between 0.1 and 0.8 (Cernusak et al., 2005; Offermann et al., 2011; Roden, Lin, & Ehleringer, 2000). The observed $\delta^{18}O_{cel}$ variability was closest to the modeled $\delta^{18}O_{cel}$ with P_{ex} values between 0.1 and 0.4. The oxygen exchange rate yielding the best match between observed and modeled $\delta^{18}O_{cel}$ was variable through the growing season. In the early growing season, modeled $\delta^{18}O_{cel}$ with P_{ex} values between 0.3 and 0.4 were closest to the $\delta^{18}O_{cel}$ measurements of EW1 and EW2 (based on small RMSE values). The $\delta^{18}O_{cel}$ measurements of FLW and SW were closest to a modeled $\delta^{18}O_{cel}$ for the summer- monsoon season, with low P_{ex} values of 0.1–0.2. At the end of the growing season, the $\delta^{18}O_{cel}$ of LW was closer to a modeled $\delta^{18}O_{cel}$ with P_{ex} values of ~0.3. Thus, the lowest modeled $\delta^{18}O_{cel}$ was for the monsoon season and is coincident with

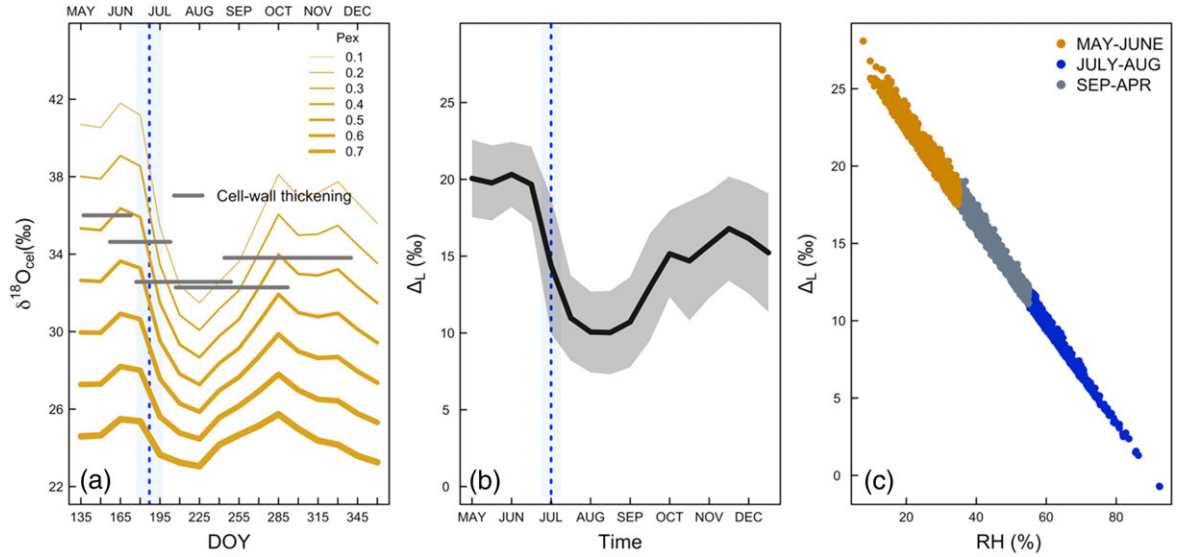

FIGURE 6 Mechanistic modeling of tree-ring cellulose $\delta^{18}O$ and leaf water enrichment Δ_L, and their sensitivities to relative humidity. (a) The Craig–Gordon model (CG) outputs are plotted from May to December, the period corresponding to cell wall thickening for all tree-ring subdivisions. The yellow color lines correspond to the CG simulations of $\delta^{18}O$ cellulose within the range of the proportion of exchangeable oxygen in cellulose (P_{ex}) variability from 0.1 (thin line) to 0.7 (thick line). The gray horizontal bars correspond to the cell wall thickening (or cell-maturation) period for each subdivision and are plotted on the mean of the $\delta^{18}O$ measurements. The cell wall thickening phase was derived from microscopic phenological observations from Morino and Hughes (University of Arizona, unpublished observations, Table S3). The climate drivers used in the CG model to make $\delta^{18}O_{cel}$ predictions were derived from PRISM data; (b) seasonal cycle of the CG mean leaf water enrichment (Δ_L). The shaded gray color corresponds to the standard deviation of modelled Δ_L. The dashed blue line in (a) and (b) indicates the average date of the monsoon onset; (c) modelled Δ_L plotted versus relative humidity (RH) in % calculated at bimonthly resolution. The Δ_L simulations were run using mean, minimum, and maximum RH. The range of RH for the hyper-arid period of May and June are plotted in orange circles. The dark blue circles represent RH range observed for the monsoon season (July–August). The gray circles correspond to the range of RH observed from September to April [Colour figure can be viewed at wileyonlinelibrary.com]

TABLE 1 Seasonal lags of xylogenesis phases between observed and modelled cellulose $\delta^{18}O$

	Enlargement	Thickening	Lag	Lag	RMSE	Mean $\delta^{18}O$	Mean $\delta^{18}O$	P_{ex}
	(1st cell)	(Duration)[2]	Enl.	Thick	(‰)	Observed	Model	
EW1	Apr 1 ± 5	May 5–June 30	4	7	1.75	36 ± 1.25	35.71 ± 1.52	0.3
EW2	May 10 ± 8	June 4–July 5	2	4	2.05	34.63 ± 1.32	34.74 ± 1.58	0.3
FLW	June 23 ± 15	July 5–Sept 15	1	10	1.86	32.56 ± 0.89	32.51 ± 1.85	0.1
SW	July 16 ± 14	August 2–Sept 30	2	8	2.09	32.28 ± 0.91	31.85 ± 1.94	0.2
LW	August 25 ± 14	Sept 13–Nov 30	2	10	1.92	33.81 ± 1.04	33.06 ± 1.82	0.3

Note. Columns are average beginning of enlargement (for the first cell in each subdivision) and average duration of cell wall thickening based on xylogenesis observations (Morino and Hughes, in preparation, see Table S3) as shown in gray bars of Figure 6; lags in weeks between onset of enlargement and onset of thickening (Enl); and time-span in weeks of secondary cell-wall thickening (thick). Root mean square error (RMSE) in ‰, the mean and standard deviation of measured and modelled cellulose $\delta^{18}O$ averaged over the duration of thickening (column 2) and corresponding rate of oxygen exchange (P_{ex}).

the FLW and SW subdivisions. The seasonal differences between early growing season (EW1 and EW2) and monsoon and post monsoon (FLW, SW, and LW) $\delta^{18}O_{cel}$ measurements is ~4‰. Similar seasonal differences were observed between EW and LW for the same species distributed across 11 sites in the US Southwest (Szejner et al., 2016). The modeled $\delta^{18}O_{cel}$ yields similar or even larger seasonal differences but only for fractional exchange rates <0.6 (Figure 6a).

Spring and early summer (May and June) were marked by higher Δ_L (Figure 6b) which decreased to the lowest enrichment during July and August and then increased in September and October. The relationship between RH and Δ_L is illustrated in Figure 6c and shows that the highest modeled Δ_L occurred during the low humidity hyperarid period (May–June) and was lowest during the monsoon season (July–August).

The $\delta^{13}C_{cel}$ and $\delta^{18}O_{cel}$ compositions of each subdivision and their correlations with climate should reflect prevailing environmental conditions during the cell wall thickening phase, when most cellulose is incorporated into the developing ring. For both isotope ratios, atmospheric VPD and the isotope ratio of winter versus summer precipitation ($\delta^{18}O_{PCP}$) are the most likely seasonally dynamic climate variables to drive intra-annual patterns in cellulose isotope composition. We used correlation analysis, focusing on observed isotope ratios and observed seasonal climate variables, to infer the best-fit seasonal

alignment. The analysis revealed a progressive seasonal and positive relationship between VPD and the $\delta^{13}C_{cel}$ and $\delta^{18}O_{cel}$ of the different tree-rings subdivisions (Figure 7). Overall, the $\delta^{18}O_{cel}$ and $\delta^{13}C_{cel}$ for the EW and FLW subdivisions were correlated to winter, spring, and early summer (June) VPD. The SW and LW subdivisions were correlated to summer (monsoon) and September VPD, although the $\delta^{18}O_{cel}$ of SW showed no correlation with VPD. The highest correlations for FLW subdivision were with May VPD for both $\delta^{13}C_{cel}$ and $\delta^{18}O_{cel}$, although some correlations were also significant with winter VPD.

4 | DISCUSSION

4.1 | Determinants of seasonality in tree-ring cellulose $\delta^{13}C$ and $\delta^{18}O$

The anatomical variability of annual growth rings results largely from seasonal interactions between climate and cambial phenology and their influences on tracheid growth and differentiation, namely, cell enlargement and secondary cell wall formation (Cuny et al., 2015; Cuny & Rathgeber, 2016; Rathgeber, Rossi, & Bontemps, 2011; Rossi et al., 2016; Vieira et al., 2015). Changes in the stable isotopic attributes in the cellulose of annual growth rings are due to progressive interactions among climate, cambial phenology, and ecophysiological processes such as photosynthetic CO_2 assimilation and stomatal conductance. Our observations revealed a consistent pattern, across 30 years, of $\delta^{13}C_{cel}$ and $\delta^{18}O_{cel}$ values with the greatest depletion in the heavier isotopes occurring in the summertime FLW, SW subdivisions, and the greatest enrichment in the heavy isotopes occurring at the earliest and latest ring boundaries in the EW and LW subdivisions. The use of a process model, started from climate–ecophysiology interactions, and conditioned on observed seasonal patterns in cambial phenology, allowed us to understand these isotope distribution patterns; they are due to the influence of seasonal phenological lags between the initial and final stages of xylogenesis.

In southern Arizona, EW production in the rings of ponderosa pine trees is initiated during the spring, typically in mid-April (Table S3) (Budelsky, 1969). The high $\delta^{13}C_{cel}$ values of the EW1 and EW2 subdivisions (Figure 4a), however, are more consistent with the use of photosynthate that is produced later in the growing season, during the hyperarid late spring or early summer period, which often extends from late May through June, and is characterized by lack of rain and extremely high air temperatures and VPD (Figure 1). Soil and atmospheric water deficits during the hyperarid period would cause reduced stomatal conductance, relative to photosynthesis rates, and thus, higher $\delta^{13}C_{cel}$ (Leavitt, 1993). Mean $\delta^{18}O_{cel}$ values in EW1 and EW2 are also high (Figure 4b) and corroborate the inferred influence of high late spring VPD on greater amounts of leaf water fractionation (Figure 6b; Farquhar et al., 2007; Szejner et al., 2016; Wright & Leavitt, 2006b). In fact, given that the starting isotope ratio of the source water is likely at a seasonal low at the time of snowmelt (Figure 3c), the fact that the ultimate EW isotope ratios reflect seasonal maxima with regard to ^{18}O enrichment indicates an extreme climatic (presumably atmospheric) pressure for evaporative fractionation during the time of secondary cell wall deposition. It is also possible that the high isotope ratios in these EW fractions are due to an alternative process—remobilization of stored carbohydrates that were assimilated and produced during the previous late summer at relatively high VPDs, characteristic of the arid postmonsoon autumn (Figure 1). This form of cross-seasonal acquisition of stored carbohydrates is known to occur and has been shown to contribute to early season cambial activity in some tree species as discussed in more detail below (Monserud & Marshall, 2001; Helle & Schleser, 2004; Kagawa, Sugimoto, & Maximov, 2006). However, our use of the CG model has revealed that in order to explain the extremely high values of $\delta^{18}O_{cel}$ in EW1 and EW2, there is no need to invoke cross-seasonal carbohydrate acquisition. We can explain most aspects of the observed isotope ratios through proper alignment of EW isotope properties with the hyperarid climate regime that most influences photosynthesis during the cell wall thickening phase of xylogenesis because cellulose deposition (cell wall thickening) lasts throughout June (Tables 1 and S3).

The initiation of FLW cells is related to the hyperarid early summer period (often referred to as the "fore-summer"), immediately preceding the onset of the monsoon (Budelsky, 1969; Griffin, Meko, Touchan, Leavitt, & Woodhouse, 2011; Leavitt, Wright, & Long, 2002). During this period, when soil moisture levels are at a minimum, turgor pressure is not high enough to maintain the levels of radial cell

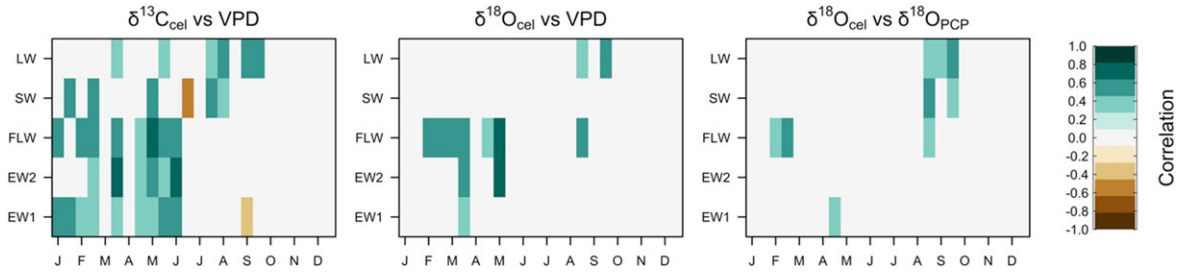

FIGURE 7 Significant Pearson correlations ($P < 0.05$) of cellulose $\delta^{13}C$ with vapor pressure deficit-VPD (left), of cellulose $\delta^{18}O$ with VPD (center) and of cellulose $\delta^{18}O$ with $\delta^{18}O$ of source water ($\delta^{18}O_{PCP}$, right). The tree-ring subdivisions (EW1, EW2, FLW, SW, and FLW) are plotted in the y-axis versus time (biweekly resolution). The VPD was calculated using PRISM data at biweekly resolution. The $\delta^{18}O$ of source water corresponds to 6-week weighted mean of precipitation $\delta^{18}O$ (see Supporting Information) with a 2-week moving window [Colour figure can be viewed at wileyonlinelibrary.com]

growth occurring during the early portion of the growing season; thus, the small cells of the FLW are formed (Gruber, Strobl, Veit, & Oberhuber, 2010). The mean $\delta^{13}C_{cel}$ and $\delta^{18}O_{cel}$ in FLW at our study site, however, suggest little influence of the seasonal soil water deficit and extremely high VPD of the fore-summer on the photosynthate used for secondary cell wall thickening (Figure 4). In water-limited forests, such as in the Mediterranean region, isotopic analyses of false rings located within EW showed high values of $\delta^{13}C_{cel}$ and inferred high iWUE (Battipaglia et al., 2014), which is clearly different from our observations. The isotope pattern in FLW cellulose in trees at our study site is likely due to the fact that although the FLW cells are indeed initiated and undergo expansion during the hyperarid period, their secondary cell walls are predominantly thickened during the moist monsoon climate system (Figure 6a, Table 1). The dominant influence of a seasonal offset between tracheid initiation and maturation, as an explanation for the observed differences between anatomy and stable isotope composition in FLW, is supported by results from the process-based isotope–climate model. The modeled values of FLW $\delta^{18}O_{cel}$ best matched observations when seasonal lags were introduced into the model to account for the entire period of monsoon cell wall thickening as an influence on FLW isotope ratios. The thickening phase for the FLW has been estimated to extend to mid-September (Figure 6a, Table 1), thus covering most of the 8- to 10-week span of the monsoon period. It is expected from theory (Equation (1) at steady state) that leaf water isotopic enrichment will be small when relative humidity is high (Craig & Gordon, 1965; Dongmann et al., 1974; Roden & Ehleringer, 2000), and a number of controlled experiments and field data have validated this relationship (Gray & Thompson, 1977; Lehmann et al., 2018; Sternberg, Mulkey, & Joseph Wright, 1989; Wright & Leavitt, 2006a). During the monsoon, higher relative humidity (or lower evaporative demand) and lower transpiration rates are associated with less enrichment of leaf water and consequently of $\delta^{18}O_{cel}$ (Figures 5a and 6c). In addition, when humidity is high, atmospheric water vapor, typically more depleted in $\delta^{18}O$ than leaf water, can diffuse into the stomatal cavity reducing leaf water enrichment (Lehmann et al., 2018).

Inconsistent with our process based model results, regression analysis of the FLW $\delta^{13}C_{cel}$ and $\delta^{18}O_{cel}$ detected that most of the interannual variance (60% and 30%, respectively) is explained by the mean VPD during the month of May (Figure 7), immediately preceding the initiation of FLW production in June. In fact, interannual variance in FLW isotope ratios is remarkably insensitive to year-to-year variation in monsoon VPD, the climate attribute that occurs annually during FLW maturation. This insensitivity is further supported in the observation of greater correlation between $\delta^{18}O_{cel}$ and monsoon $\delta^{18}O_{PCP}$ (Figure 7), suggesting that the FLW $\delta^{18}O_{cel}$ is reflecting monsoon source water, not variance in VPD. Having concluded that the FLW $\delta^{18}O_{cel}$ is most consistent with the utilization of photosynthate produced during the monsoon period, how do we explain the significant interannual correlation between spring hydroclimate and FLW $\delta^{18}O_{cel}$, but not monsoon hydroclimate?

In explaining this paradox, we considered two possible causes. It is possible that Δ_L decreased because Δ_v was high and thus when w_a/w_i decreased, it also decreased Δ_L. This explanation would be consistent with isotopically enriched precipitation and therefore enriched atmospheric water vapor, as seasonal temperatures warmed in the early summer. We do not favor this cause, despite its simplicity and direct nature, because although FLW $\delta^{18}O_{cel}$ is indeed low, our observations revealed that most of the FLW cellulose was produced considerably later in the summer, well outside the direct seasonal effect of May climate and during the monsoon period when VPD decreases at the same time that Δ_v increases. Furthermore, although an early summer increase in both Δ_v and VPD could explain the suppression of Δ_L, it does not lend itself to an explanation of the significant interannual correlation between the FLW $\delta^{18}O_{cel}$ and variance in May climate. However, we acknowledge that we do not have direct observations of Δ_v, which imposes a challenge to further direct evaluations of this possible cause. These observations are needed to fully evaluate possible seasonal influences of Δ_v.

A second possible cause, which we favor at the moment, is that although most of the photosynthate used in cellulose synthesis for FLW cell wall thickening is produced during the wetter monsoon period in midsummer, some photosynthate is likely allocated from accumulated carbohydrate pools produced during the spring and early summer. Past studies with *P. ponderosa* and *P. contorta* have shown that low molecular weight sugars can accumulate in woody tissues during drought (Piper, Fajardo, & Hoch, 2017), and in *P. halepensis* during seasonal transitions from wetter springs to drier summers (Klein, Hoch, Yakir, & Körner, 2014). These accumulations are presumably due to imbalances between the supply and demand of photosynthate (Hoch, 2015; Körner, 2003), triggered by geographic or seasonal changes in cambial sink limitations (Sala, Woodruff, & Meinzer, 2012), respectively. In our study, the likely accumulation of sugars in xylem parenchyma as drought conditions gradually worsen in May and June (hyperarid and premonsoon) could explain the significant correlation between FLW $\delta^{18}O_{cel}$ and interannual variation in May climate. FLW cell enlargement occurs in late June with cell maturation beginning on July 5 ± 10 days (Table S3), concurrent with the beginning of the summer monsoon. Consequently, the FLW $\delta^{18}O_{cel}$ should carry a monsoon signal, unless stored sugars are also incorporated.

A transition from use of accumulated sugars to current photosynthate with the onset of monsoon rains in July, the principal season of secondary cell wall formation, would explain why the CG model was best at predicting FLW $\delta^{18}O_{cel}$ when conditioned with monsoon climate variables. The lack of a significant correlation between FLW $\delta^{18}O_{cel}$ and interannual variation in monsoon climate, during July and August, is likely due to low $^{18}O/^{16}O$ fractionation potential in the face of consistently higher RH (lower VPD).

Significant correlations were also found for FLW $\delta^{18}O_{cel}$ against $\delta^{18}O_{PCP}$ after the middle of July through the end of August (Figure 7) roughly indicating the transition from the use of the accumulated (springtime) carbohydrates to carbohydrates produced during the later monsoon.

Tracheids initiated after the monsoon onset, developed into a band of larger thin-walled cells that we have called SW. The SW mean $\delta^{13}C_{cel}$ and $\delta^{18}O_{cel}$ values are indicative of relatively low iWUE (Figure S4) and evaporative enrichment, respectively, presumably because the photosynthate used during the maturation of SW tracheids is produced during the relatively wet period of the monsoon. This is further indicated by the high correlation between $\delta^{18}O_{cel}$ and

$\delta^{18}O_{PCP}$ and its insensitivity to interannual variation in monsoon VPD (Figure 7). Isotopically, SW cells are similar to FLW cells.

In contrast to SW and FLW, LW cells were initiated in September and they have $\delta^{13}C_{cel}$ and $\delta^{18}O_{cel}$ values indicative of higher VPD influences, suggesting that while the cells were produced during the monsoon, most cell wall thickening occurred during the climatically variable late monsoon and dry postmonsoon period and probably extended into November (Table 1). Note also that the LW $\delta^{18}O_{cel}$ correlations against $\delta^{18}O_{PCP}$ are significant for the late monsoon and postmonsoon periods (Figure 7), suggesting exchange during cellulose synthesis, but perhaps also the influence of VPD on secondary evaporation of precipitation, and therefore on source water, as it falls through the drier post monsoon atmosphere. In the drier postmonsoon period, seasonal hydroclimate may exhibit interannual variance that leads to periodic water-stress to needle gas-exchange processes and forces detectable correlations with the cellulose isotope ratios of LW.

4.2 | Seasonal variations of postassimilation oxygen exchange rate (P_{ex})

The fraction of exchanged oxygen atoms during cellulose synthesis, P_{ex}, has most often been considered as constant, around a mean value of 0.42 (42%), among species and in trees of the same species from different growth conditions (Barbour et al., 2004; Cernusak et al., 2005; Farquhar & Cernusak, 2005; Roden et al., 2000; Sternberg & Ellsworth, 2011). A few studies, however, have found variable P_{ex} throughout the growing season and across geospatial aridity gradients (Cheesman & Cernusak, 2016; Gessler et al., 2009; Offermann et al., 2011). The natural abundance of ^{18}O in carbohydrates due to variability in the isotopic ratios of source water may explain part of this variability (Yakir, 1992), though much of the variation is likely caused by environmental influences on the exchange of ^{18}O between photosynthate and xylem water during cellulose biosynthesis. In a study of European beech species from a temperate forest, Offerman et al. (2011) found that P_{ex} decreased through the season, from spring to midsummer (0.76 to ~0). Variable P_{ex} was also observed across an aridity gradient in Eucalyptus trees in Australia (Cheesman & Cernusak, 2016). In that study, greater P_{ex} was observed in arid sites (~0.68), compared with wetter sites (~0.21). These past reported changes in environmental water availability, and their influences on P_{ex}, are consistent with our modelled estimates of P_{ex}, which were higher during the drier late spring and early summer (reflected in EW1 and EW2), lower during the wetter monsoon period (reflected in FLW and SW and partially in LW), and higher again during the drier postmonsoon period (reflected in LW).

The total proportion of oxygen atoms available for exchange between those in phloem-transported sucrose and xylem water depends on the number of cycles that pass through a triose phosphate phase during cellulose synthesis (Hill, Waterhouse, Field, Switsur, & Ap Rees, 1995). The extent of triose-phosphate cycling depends, in turn, on the sucrose turnover time during cellulose synthesis (Barbour & Farquhar, 2000), that is, how fast available sucrose is transported from the phloem and used for cellulose synthesis. Song, Farquhar, Gessler, and Barbour (2014) showed that a positive relationship exists between P_{ex} and the turnover time of the nonstructural carbohydrate (NSC) pool available for cellulose synthesis. The increasing turnover time itself is caused by a larger NSC pool size at the site of cellulose synthesis in relation to fluxes in and out of the pool (Barbour & Farquhar, 2000). Variations in P_{ex} as a function of available moisture (or aridity) whether intraseasonal (our study site) or across a geospatial gradient (Cheesman & Cernusak, 2016) might be associated with the role of water availability on NSC pool-size dynamics. At our site, we expect that water stress causes changes in NSC pool dynamics at many points along the path between needle photosynthesis and cambial cellulose synthesis. This could occur by reducing net photosynthesis rate, influencing the partitioning of photoassimilates between mesophyll and phloem cells, changing phloem transport rates, and/or reducing the rate of cellulose synthesis.

The value of P_{ex} has the potential to influence conclusions about the relative roles of source water and atmospheric VPD in determining isotope–climate interactions. Theoretically, observed $\delta^{18}O_{cel}$ values reflect combined influences from the source water ($\delta^{18}O_{PCP}$) and leaf water fractionation (Δ_L). At P_{ex} > 0.6, the $\delta^{18}O_{cel}$ seasonal variance is damped ~2‰, compared with the ~4‰ observed for P_{ex} < 0.6 (Figure 6A), confirming that our conclusion of a dominant role for VPD on observed $\delta^{18}O_{cel}$ values, is dependent on an assumption of P_{ex} at the lower end of possible values. Without consideration of the possible use of older photoassimilates, our modeling of predicted $\delta^{18}O_{cel}$ values is most consistent with lower estimates of P_{ex} (10–40%; Figure 6a). The higher values of P_{ex} were predicted to occur during the early- and late-growing seasons, compared with the monsoon season. This modeling result indicates that although a smaller fraction of oxygen originates from needle water during the early- and late-growing season, the fraction is still high enough to allow a dominant control by VPD as the primary hydroclimate signal recorded in $\delta^{18}O_{cel}$, not that of source water. Conversely, despite recording a larger fraction of oxygen from needle water in the $\delta^{18}O_{cel}$ signal during the monsoon, low evaporative enrichment, high soil moisture conditions, and greater molecular exchange between the ambient air and stomatal cavities during this season yielded $\delta^{18}O_{cel}$ values closer to source water.

Our studies have shown that the distinct seasonal cycles of $\delta^{13}C$ and $\delta^{18}O$ observed in successive anatomical zones of individual tree rings of *P. ponderosa* are strongly influenced by seasonal variations in evaporative demand. Process-based model predictions of the $\delta^{18}O_{cel}$ pattern were consistent with observations, with the accuracy determined mostly by the proportion of the postassimilation oxygen exchange rate. The distribution of stable isotopes in specific tree-ring subdivisions was best explained when seasonal lags of xylogenesis phases were taken into account. This insight points to the relevance of aligning tree-ring formation phenology, isotope fractionation processes, and associated climate drivers to better understand the present and past seasonal progression of isotope–climate relations and forest–climate interactions.

ACKNOWLEDGEMENTS

This study was supported by a grant from the Macrosystems program in the Emerging Frontiers section of the U.S. National Science Foundation (NSF award 1065790) and the Ecosystems Program in the Division of Environmental Biology (NSF Award 1754430). We

would like to thank C. Niel, A. Thomas, L. Wells, F. Moreno, M. Twitty, A. Spencer, C. Monteleone, and E. Bergman for their assistance in tree-ring and cellulose sample processing. We thank the two anonymous reviewers for their valuable comments.

CONFLICT OF INTERESTS

The authors have no conflict of interest to declare.

ORCID

Soumaya Belmecheri http://orcid.org/0000-0003-1258-2741

REFERENCES

Adams, D. K., & Comrie, A. C. (1997). The North American monsoon. *Bulletin of the American Meteorological Society*, *78*, 2197–2213.

Babst, F., Wright, W. E., Szejner, P., Wells, L., Belmecheri, S., & Monson, R. K. (2016). Blue intensity parameters derived from ponderosa pine tree rings characterize intra-annual density fluctuations and reveal seasonally divergent water limitations. *Trees*, *30*, 1403–1415.

Barbour, M. M., & Farquhar, G. D. (2000). Relative humidity- and ABA-induced variation in carbon and oxygen isotope ratios of cotton leaves. *Plant, Cell and Environment*, *23*, 473–485.

Barbour, M. M., Roden, J. S., Farquhar, G. D., & Ehleringer, J. R. (2004). Expressing leaf water and cellulose oxygen isotope ratios as enrichment above source water reveals evidence of a Péclet effect. *Oecologia*, *138*, 426–435.

Barbour, M. M., Schurr, U., Henry, B. K., Wong, S. C., & Farquhar, G. D. (2000). Variation in the oxygen isotope ratio of phloem sap sucrose from castor bean. Evidence in support of the Péclet Effect. *Plant Physiology*, *123*, 671 LP–680.

Barbour, M. M., Walcroft, A. S., & Farquhar, G. D. (2002). Seasonal variation in $\delta^{13}C$ and $\delta^{18}O$ of cellulose from growth rings of Pinus radiata. *Plant, Cell & Environment*, *25*, 1483–1499.

Battipaglia, G., Campelo, F., Vieira, J., Grabner, M., De Micco, V., Nabais, C., … de Luis, M. (2016). Structure and function of intra–annual density fluctuations: Mind the gaps. *Frontiers in Plant Science*, *7*, 595.

Battipaglia, G., De Micco, V., Brand, W., Saurer, M., Aronne, G., Linke, P., & Cherubini, P. (2014). Drought impact on water use efficiency and intra-annual density fluctuations in Erica arborea on Elba (Italy). *Plant, Cell & Environment*, *37*, 382–391.

Budelsky, C. A. (1969). *Variation in transpiration and its relationship with growth for Pinus ponderosa Lawson in southern Arizona*. UNiversity of Arizona.

Campelo, F., Gutiérrez, E., Ribas, M., Nabais, C., & Freitas, H. (2007). Relationships between climate and double rings in Quercus ilex from northeast Spain. *Canadian Journal of Forest Research*, *37*, 1915–1923.

Cernusak, L. A., Barbour, M. M., Arndt, S. K., Cheesman, A. W., English, N. B., Feild, T. S., … Farquhar, G. D. (2016). Stable isotopes in leaf water of terrestrial plants. *Plant, Cell & Environment*, 1087–1102, *39*.

Cernusak, L. A., Farquhar, G. D., & Pate, J. S. (2005). Environmental and physiological controls over oxygen and carbon isotope composition of Tasmanian blue gum, Eucalyptus globulus. *Tree Physiology*, *25*, 129–146.

Cheesman, A. W., & Cernusak, L. A. (2016). Infidelity in the outback: Climate signal recorded in $\Delta^{18}O$ of leaf but not branch cellulose of eucalypts across an Australian aridity gradient (ed Meinzer F). *Tree Physiology*, *37*, 554–564.

Craig, H., & Gordon, L. (1965). Deuterium and oxygen 18 variations in the ocean and the marine. *Atmosphere*, 9–130.

Cuntz, M., Ogee, J., Farquhar, G. D., Peylin, P., & Cernusak, L. A. (2007). Modelling advection and diffusion of water isotopologues in leaves. *Plant, Cell & Environment*, *30*, 892–909.

Cuny, H. E., & Rathgeber, C. B. K. (2016). Xylogenesis: Coniferous trees of temperate forests are listening to the climate tale during the growing season but only remember the last words! *Plant Physiology*, *171*, 306 LP–317.

Cuny, H. E., Rathgeber, C. B. K., Frank, D., Fonti, P., Mäkinen, H., Prislan, P., … Fournier, M. (2015). Woody biomass production lags stem-girth increase by over one month in coniferous forests. *Nature Plants*, *1*, 15160.

Cuny, H. E., Rathgeber, C. B. K., Kiessé, T. S., Hartmann, F. P., Barbeito, I., & Fournier, M. (2013). Generalized additive models reveal the intrinsic complexity of wood formation dynamics. *Journal of Experimental Botany*, *64*, 1983–1994.

Daly, C., Halbleib, M., Smith, J. I., Gibson, W. P., Doggett, M. K., Taylor, G. H., … Pasteris, P. P. (2008). Physiographically sensitive mapping of climatological temperature and precipitation across the conterminous United States. *International Journal of Climatology*, *28*, 2031–2064.

De Micco, V., Balzano, A., Čufar, K., Aronne, G., Gričar, J., Merela, M., & Battipaglia, G. (2016). Timing of false ring formation in Pinus halepensis and Arbutus unedo in Southern Italy: Outlook from an analysis of xylogenesis and tree-ring chronologies. *Frontiers in Plant Science*, *7*, 1–14.

Deslauriers, A., Rossi, S., Anfodillo, T., & Saracino, A. (2008). Cambial phenology, wood formation and temperature thresholds in two contrasting years at high altitude in southern Italy. *Tree Physiology*, *28*, 863–871.

Dongmann, G., Nurnberg, H. W., Forstel, H., & Wagener, K. (1974). On the enrichment of H2 ^{18}O in the leaves of transpiring plants. *Radiation and Environmental Biophysics*, *11*, 41–52.

Eastoe, C. J., & Dettman, D. L. (2016). Isotope amount effects in hydrologic and climate reconstructions of monsoon climates: Implications of some long-term data sets for precipitation. *Chemical Geology*, *430*, 78–89.

Evans, M. N., Selmer, K. J., Breeden, B. T., Lopatka, A. S., & Plummer, R. E. (2016). Correction algorithm for online continuous flow $\delta^{13}C$ and $\delta^{18}O$ carbonate and cellulose stable isotope analyses. *Geochemistry, Geophysics, Geosystems*, *17*, 3580–3588.

Farquhar, G., Barbour, M., & Henry, B. (1998). Interpretation of oxygen isotope composition of leaf material. In H. Griffiths (Ed.), *Stable Isotopes: Integration of Biological, Ecological, and Geochemical Processes* (pp. 27–61). BIOS Scientific Publishers Ltd.

Farquhar, G. D., & Cernusak, L. A. (2005). On the isotopic composition of leaf water in the non-steady state. *Functional Plant Biology*, *32*, 293–303.

Farquhar, G. D., Cernusak, L. A., & Barnes, B. (2007). Heavy water fractionation during transpiration. *Plant Physiology*, *143*. 11 LP-18

Farquhar, G. D., Hubick, K. T., Condon, A. G., & Richards, R. A. (1989a). In P. W. Rundel, J. R. Ehleringer, & K. A. Nagy (Eds.), *Carbon isotope fractionation and plant water-use efficiency* (pp. 21–40). New York, NY: Springer New York.

Farquhar, G. D., Hubick, K. T., Condon, A. G., & Richards, R. A. (1989b). In P. W. Rundel, J. R. Ehleringer, & K. A. Nagy (Eds.), *Carbon isotope fractionation and plant water-use efficiency BT—Stable isotopes in ecological research* (pp. 21–40). New York, NY: Springer New York.

Farquhar, G. D., & Lloyd, J. (1993). *Carbon and oxygen isotope effects in the exchange of carbon dioxide between terrestrial plants and the atmosphere BT—Stable isotopes and plant carbon-water relations*. (pp. 47–70). San Diego: Academic Press.

Frank, D. C., Poulter, B., Saurer, M., Esper, J., Huntingford, C., Helle, G., … Weigl, M. (2015). Water-use efficiency and transpiration across European forests during the Anthropocene. *Nature Climate Change*, *5*, 579–583.

Fritts, H. C. (1976). *Tree rings and climate* (p. 567). San Diego: Academic Press.

Fritts, H. C., Vaganov, E. A., Sviderskaya, I. V., & Shashkin, A. V. (1991). Climatic variation and tree-ring structure in conifers: empirical and mechanistic models of tree-ring width, number of cells, cell size, cell-wall thickness and wood density. *Climate Research*, *1*, 97–116.

Gessler, A., Brandes, E., Buchmann, N., Helle, G., Rennenberg, H., & Barnard, R. L. (2009). Tracing carbon and oxygen isotope signals from newly assimilated sugars in the leaves to the tree-ring archive. *Plant, Cell & Environment*, *32*, 780–795.

Gessler, A., Brandes, E., Keitel, C., Boda, S., Kayler, Z. E., Granier, A., … Treydte, K. (2013). The oxygen isotope enrichment of leaf-exported assimilates—Does it always reflect lamina leaf water enrichment? *New Phytologist*, *200*, 144–157.

Gessler, A., Ferrio, J. P., Hommel, R., Treydte, K., Werner, R. A., & Monson, R. K. (2014). Stable isotopes in tree rings: Towards a mechanistic understanding of isotope fractionation and mixing processes from the leaves to the wood. *Tree Physiology*, *34*, 796–818.

Graham, R. T., & Jain, T. B. (2005). Ponderosa Pine. *Ecosystems*, *1*, 1–32.

Gray, J., & Thompson, P. (1977). Climatic information from $^{18}O/^{16}O$ analysis of cellulose, lignin and whole wood from tree rings. *Nature*, *270*, 708–709.

Green, J. W. (1963). *Wood cellulose Methods in Carbohydrate Chemistry: vol 3* (pp. 9–21). New York: Academic Press.

Griffin, D., Meko, D. M., Touchan, R., Leavitt, S. W., & Woodhouse, C. A. (2011). Latewood chronology development for summer-moisture reconstruction in the US Southwest. *Tree-Ring Research*, *67*, 87–101.

Griffin, D., Woodhouse, C. A., Meko, D. M., Stahle, D. W., Faulstich, H. L., Carrillo, C., … Leavitt, S. W. (2013). North American monsoon precipitation reconstructed from tree-ring latewood. *Geophysical Research Letters*, *40*, 954–958.

Gruber, A., Strobl, S., Veit, B., & Oberhuber, W. (2010). Impact of drought on the temporal dynamics of wood formation in Pinus sylvestris. *Tree Physiology*, *30*, 490–501.

Helle, G., & Schlesser, G. H. (2004). Beyond CO2-fixation by Rubisco—An interpretation of $^{13}C/^{12}C$ variations in tree rings from novel intra-seasonal studies on broad-leaf trees. *Plant, Cell and Environment*, *27*, 367–380.

Helliker, B. R., & Ehleringer, J. R. (2002). Differential ^{18}O enrichment of leaf cellulose in C3 versus C4 grasses. *Functional Plant Biology*, *29*, 435–442.

Higgins, R. W., Yao, Y., & Wang, X. L. (1997). Influence of the North American Monsoon System on the U.S. Summer Precipitation Regime. *Journal of Climate*, *10*, 2600–2622.

Hill, S. A., Waterhouse, J. S., Field, E. M., Switsur, V. R., & Ap Rees, T. (1995). Rapid recycling of triose phosphates in oak stem tissue. *Plant, Cell & Environment*, *18*, 931–936.

Hoch, G. (2015). *Carbon reserves as indicators for carbon limitation in trees BT—Progress in Botany: Vol. 76. (eds Lüttge U, Beyschlag W)*. (pp. 321–346). Cham: Springer International Publishing.

Hu, H., & Dominguez, F. (2014). Evaluation of oceanic and terrestrial sources of moisture for the North American monsoon using numerical models and precipitation stable isotopes. *Journal of Hydrometeorology*, *16*, 19–35.

Kagawa, A., Sugimoto, A., & Maximov, T. C. (2006). Seasonal course of translocation, storage and remobilization of ^{13}C pulse-labeled photoassimilate in naturally growing Larix gmelinii saplings. *New Phytologist*, *171*, 793–804.

Kahmen, A., Simonin, K., Tu, K. P., Merchant, A., Callister, A., Siegwolf, R., … Arndt, S. K. (2008). Effects of environmental parameters, leaf physiological properties and leaf water relations on leaf water $\delta^{18}O$ enrichment in different Eucalyptus species. *Plant, Cell & Environment*, *31*, 738–751.

Keeling, C. D., Piper, S. C., Bacastow, R. B., Wahlen, M., Whorf, T. P., Heimann, M., & Meijer, H. A. (2005). Atmospheric CO_2 and $^{13}CO_2$ exchange with the terrestrial biosphere and oceans from 1978 to 2000: Observations and carbon cycle implications. In I. T. Baldwin, M. M. Caldwell, G. Heldmaier, R. B. Jackson, O. L. Lange, H. A. Mooney, et al. (Eds.), *A history of atmospheric CO_2 and its effects on plants, animals, and ecosystems* (pp. 83–113). New York: Springer-Verlag.

Klein, T., Hoch, G., Yakir, D., & Körner, C. (2014). Drought stress, growth and nonstructural carbohydrate dynamics of pine trees in a semi-arid forest. *Tree Physiology*, *34*, 981–992.

Körner, C. (2003). Carbon limitation in trees. *Journal of Ecology*, *91*, 4–17.

Lachenbruch, B., & McCulloh, K. A. (2014). Traits, properties, and performance: How woody plants combine hydraulic and mechanical functions in a cell, tissue, or whole plant. *New Phytologist*, *204*, 747–764.

Laumer, W., Andreu, L., Helle, G., Schleser, G. H., Wieloch, T., & Wissel, H. (2009). A novel approach for the homogenization of cellulose to use micro-amounts for stable isotope analyses. *Rapid Communications in Mass Spectrometry*, *23*, 1934–1940.

Leavitt, S. W. (1993). Environmental information from $^{13}C/^{12}C$ ratios of wood. In: *Climate change in continental isotopic records*, (pp. 325–331). American Geophysical Union.

Leavitt, S. W., Woodhouse, C. A., Castro, C. L., Wright, W. E., Meko, D. M., Touchan, R., … Ciancarelli, B. (2011). The North American monsoon in the U.S. Southwest: Potential for investigation with tree-ring carbon isotopes. *Quaternary International*, *235*, 101–107.

Leavitt, S. W., Wright, W. E., & Long, A. (2002). Spatial expression of ENSO, drought, and summer monsoon in seasonal $\delta^{13}C$ of ponderosa pine tree rings in southern Arizona and New Mexico. *Journal of Geophysical Research-Atmospheres*, *107*, 4349.

Lehmann, M. M., Goldsmith, G. R., Schmid, L., Gessler, A., Saurer, M., & Siegwolf, R. T. W. (2018). The effect of ^{18}O-labelled water vapour on the oxygen isotope ratio of water and assimilates in plants at high humidity. *New Phytologist*, *217*, 105–116.

Loucos, K. E., Simonin, K. A., Song, X., & Barbour, M. M. (2015). Observed relationships between leaf $H_2{}^{18}O$ Péclet effective length and leaf hydraulic conductance reflect assumptions in Craig–Gordon model calculations. *Tree Physiology*, *35*, 16–26.

Majoube, M. (1970). Fractionation Factor of ^{18}O between Water Vapour and Ice. *Nature*, *226*, 1242.

McCarroll, D., Gagen, M. H., Loader, N. J., Robertson, I., Anchukaitis, K. J., Los, S., … Waterhousee, J. S. (2009). Correction of tree ring stable carbon isotope chronologies for changes in the carbon dioxide content of the atmosphere. *Geochimica et Cosmochimica Acta*, *73*, 1539–1547.

McCarroll, D., & Loader, N. J. (2004). Stable isotopes in tree rings. *Quaternary Science Reviews*, *23*, 771–801.

McDowell, N. G., White, S., & Pockman, W. T. (2008). Transpiration and stomatal conductance across a steep climate gradient in the southern Rocky Mountains. *Ecohydrology*, *1*, 193–204.

Meko, D. M., & Baisan, C. H. (2001). Pilot study of latewood-width of conifers as an indicator of variability of summer rainfall in the North American monsoon region. *International Journal of Climatology*, *21*, 697–708.

Monserud, R. A., & Marshall, J. D. (2001). Time-series analysis of $\delta^{13}C$ from tree rings. I. Time trends and autocorrelation. *Tree Physiology*, *21*, 1087–1102.

Offermann, C., Ferrio, J. P., Holst, J., Grote, R., Siegwolf, R., Kayler, Z., & Gessler, A. (2011). The long way down—Are carbon and oxygen isotope signals in the tree ring uncoupled from canopy physiological processes? *Tree Physiology*, *31*, 1088–1102.

Ogée, J., Barbour, M. M., Wingate, L., Bert, D., Bosc, A., Stievenard, M., … Dewar, R. C. (2009). A single-substrate model to interpret intra-annual stable isotope signals in tree-ring cellulose. *Plant, Cell & Environment*, *32*, 1071–1090.

Pflug, E. E., Siegwolf, R., Buchmann, N., Dobbertin, M., Kuster, T. M., Günthardt-Goerg, M. S., & Arend, M. (2015). Growth cessation uncouples isotopic signals in leaves and tree rings of drought-exposed oak trees. *Tree Physiology*, *35*, 1095–1105.

Piper, F. I., Fajardo, A., & Hoch, G. (2017). Single-provenance mature conifers show higher non-structural carbohydrate storage and reduced growth in a drier location. *Tree Physiology*, *37*, 1001–1010.

Rathgeber, C. B. K., Cuny, H. E., & Fonti, P. (2016). Biological basis of tree-ring formation: A crash course. *Frontiers in Plant Science*, *7*, 1–7.

Rathgeber, C. B. K., Rossi, S., & Bontemps, J.-D. (2011). Cambial activity related to tree size in a mature silver-fir plantation. *Annals of Botany*, *108*, 429–438.

Roden, J., Kahmen, A., Buchmann, N., & Siegwolf, R. (2015). The enigma of effective path length for ^{18}O enrichment in leaf water of conifers. *Plant, Cell & Environment*, *38*, 2551–2565.

Roden, J. S., & Ehleringer, J. R. (1999). Hydrogen and oxygen isotope ratios of tree-ring cellulose for riparian trees grown long-term under hydroponically controlled environments. *Oecologia*, *121*, 467–477.

Roden, J. S., & Ehleringer, J. R. (2000). Hydrogen and oxygen isotope ratios of tree ring cellulose for field-grown riparian trees. *Oecologia*, *123*, 481–489.

Roden, J. S., & Ehleringer, J. R. (2007). Summer precipitation influences the stable oxygen and carbon isotopic composition of tree-ring cellulose in Pinus ponderosa. *Tree Physiology*, *27*, 491–501.

Roden, J. S., Johnstone, J. A., & Dawson, T. E. (2009). Intra-annual variation in the stable oxygen and carbon isotope ratios of cellulose in tree rings of coast redwood (Sequoia sempervirens). *The Holocene*, *19*, 189–197.

Roden, J. S., Lin, G., & Ehleringer, J. R. (2000). A mechanistic model for interpretation of hydrogen and oxygen isotope ratios in tree-ring cellulose. *Geochimica et Cosmochimica Acta*, *64*, 21–35.

Rossi, A., Anfodillo, T., Čufar, K., Cuny, H. E., Deslauriers, A., Fonti, P., … Treml, V. (2016). Pattern of xylem phenology in conifers of cold ecosystems at the Northern Hemisphere. *Global Change Biology*, *22*, 3804–3813.

Rossi, S., Anfodillo, T., & Deslauriers, A. (2006). Assessment of cambial activity and xylogenesis by microsampling tree species: An example at the Alpine Timberline. *IAWA Journal*, *27*, 383–394.

Rossi, S., Deslauriers, A., & Morin, H. (2003). Application of the Gompertz equation for the study of xylem cell development. *Dendrochronologia*, *21*, 33–39.

Rossi, S., Morin, H., & Deslauriers, A. (2012). Causes and correlations in cambium phenology: Towards an integrated framework of xylogenesis. *Journal of Experimental Botany*, *63*, 2117–2126.

Sala, A., Woodruff, D. R., & Meinzer, F. C. (2012). Carbon dynamics in trees: Feast or famine? *Tree Physiology*, *32*, 764–775.

Sarris, D., Siegwolf, R., & Körner, C. (2013). Inter- and intra-annual stable carbon and oxygen isotope signals in response to drought in Mediterranean pines. *Agricultural and Forest Meteorology*, *168*, 59–68.

Saurer, M., Spahni, R., Frank, D. C., Joos, F., Leuenberger, M., Loader, N. J., … Young, G. H. F. (2014). Spatial variability and temporal trends in water-use efficiency of European forests. *Global Change Biology*, *20*, 3700–3712.

Sheppard, P., Comrie, A., Packin, G., Angersbach, K., & Hughes, M. (2002). The climate of the US Southwest. *Climate Research*, *21*, 219–238.

Song, X., Loucos, K. E., Simonin, K. A., Farquhar, G. D., & Barbour, M. M. (2015). Measurements of transpiration isotopologues and leaf water to assess enrichment models in cotton. *New Phytologist*, *206*, 637–646.

Song, X., Farquhar, G. D., Gessler, A., & Barbour, M. M. (2014). Turnover time of the non-structural carbohydrate pool influences $\delta^{18}O$ of leaf cellulose. *Plant, Cell & Environment*, *37*, 2500–2507.

Song, X. I. N., Barbour, M. M., Farquhar, G. D., Vann, D. R., & Helliker, B. R. (2013). Transpiration rate relates to within- and across-species variations in effective path length in a leaf water model of oxygen isotope enrichment. *Plant, Cell & Environment*, *36*, 1338–1351.

Sternberg, L., & Ellsworth, P. F. V. (2011). Divergent biochemical fractionation, not convergent temperature, explains cellulose oxygen isotope enrichment across latitudes. *PLoS One*, *6*. e28040

Sternberg, L., Mulkey, S. S., & Joseph Wright, S. (1989). Oxygen isotope ratio stratification in a tropical moist forest. *Oecologia*, *81*, 51–56.

Sternberg, L., Pinzon, M. C., Anderson, W. T., & Jahren, A. H. (2006). Variation in oxygen isotope fractionation during cellulose synthesis: Intramolecular and biosynthetic effects. *Plant, Cell & Environment*, *29*, 1881–1889.

Sternberg, L. D. S. L., Deniro, M. J., & Savidge, R. A. (1986). Oxygen isotope exchange between metabolites and water during biochemical reactions leading to cellulose synthesis. *Plant Physiology*, *82*, 423 LP–427.

Stokes, M. A., & Smiley, T. L. (1996). *An Introduction to Tree-Ring Dating*. Tucson, Arizona, USA: The University of Arizona Press.

Szejner, P., Wright, W. E., Babst, F., Belmecheri, S., Trouet, V., Leavitt, S. W., … Monson, R. K. (2016). Latitudinal gradients in tree ring stable carbon and oxygen isotopes reveal differential climate influences of the North American Monsoon System. *Journal of Geophysical Research – Biogeosciences*, *121*, 1978–1991.

Vaganov, E. A., Anchukaitis, K. J., & Evans, M. N. (2011). In M. K. Hughes, T. W. Swetnam, & H. F. Diaz (Eds.), *How well understood are the processes that create dendroclimatic records? A mechanistic model of the climatic control on conifer tree-ring growth dynamics* (pp. 37–75). Dordrecht: Springer Netherlands.

Vaganov, E. A., Hughes, M. K., & Shashkin, A. V. (2006). *Growth dynamics of conifer tree rings* (Vol. 183). Berlin/Heidelberg: Springer-Verlag.

Vieira, J., Campelo, F., Rossi, S., Carvalho, A., Freitas, H., & Nabais, C. (2015). Adjustment Capacity of Maritime Pine Cambial Activity in Drought-Prone Environments. *PLoS One*, *10*, e0126223.

Wright, W. E. (2001). Delta-deuterium and delta-oxygen-18 in mixed conifer systems in the United States southwest: The potential of delta-oxygen-18 in Pinus ponderosa tree rings as a natural environmental recorder, Vol. PhD. University of Arizona.

Wright, W.E., Leavitt, S. W. (2006a). Boundary layer humidity reconstruction for a semiarid location from tree ring cellulose $\delta^{18}O$. *Journal of Geophysical Research-Atmospheres*, *111*, 1–9.

Wright, W. E., & Leavitt, S. W. (2006b). Needle cell elongation and maturation timing derived from pine needle cellulose $\delta^{18}O$. *Plant, Cell and Environment*, *29*, 1–14.

Yakir, D. (1992). Variations in the natural abundance of oxygen-18 and deuterium in plant carbohydrates. *Plant, Cell & Environment*, *15*, 1005–1020.

SUPPORTING INFORMATION

Additional supporting information may be found online in the Supporting Information section at the end of the article.

How to cite this article: Belmecheri S, Wright WE, Szejner P, Morino KA, Monson RK. Carbon and oxygen isotope fractionations in tree rings reveal interactions between cambial phenology and seasonal climate. *Plant Cell Environ*. 2018;41: 2758–2772. https://doi.org/10.1111/pce.13401